A NONLINEAR EQUALIZATION ALGORITHM FOR SINGLE-CARRIER BLOCK TRANSMISSION SYSTEMS

Shih-Jung Wang, Jiun-Jie Jia, Kuei-Chiang Lai, and Szu-Lin Su

Department of Electrical Engineering, National Cheng Kung University, Taiwan, R.O.C.

ABSTRACT

Combating the intersymbol interference is an important issue in single-carrier block transmission systems. In this paper, we present a nonlinear equalizer that combines frequency-domain (FD) prefiltering with time-domain tree search detection. Simulation results show that the proposed algorithm achieves a detection performance that is very close to that of the conventional tree search equalizer (which employs the QRD-M algorithm), but with a much lower complexity. In addition, the proposed algorithm performs significantly better than the linear equalizers and decision-feedback equalizers, with only a modest increase in complexity.

Index Terms— Single-carrier block transmission, equalization, prefilter, frequency-domain processing, tree search

1. INTRODUCTION

As the data rates of broadband wireless communication systems are pushed increasingly higher, intersymbol interference (ISI) has become a key impairment to system performance. Among the approaches intended to address this issue, single-carrier block transmission (SCBT) is a promising technique that is very suitable for *uplink* transmission, due to the following reasons [1]. First, compared with orthogonal frequency division multiplexing (OFDM), SCBT has a lower peak-to-average power ratio, and is less sensitive to radio-frequency impairments. Second, SCBT has a block structure similar to that of OFDM, thereby allowing for frequency-domain equalization (FDE), which is much more efficient than the time-domain (TD) equalization counterparts in typical system settings.

In SCBT systems, modulation symbols are grouped into data blocks. The guard time (GT) is then inserted between adjacent data blocks in order to avoid interblock interference (IBI). Depending on the contents of the GTs, SCBT can be divided into two major categories. The first is the cyclic-prefix SCBT (CP-SCBT), for which the tail of each data block is copied over to fill in the GT in front of the respective block, in a manner similar to the CP of the OFDM systems. The second is the training sequence-aided SCBT (TA-SCBT), for which each GT is filled with a fixed training sequence (TS). Since the presence of TS facilitates synchronization and channel estimation at little loss of data rate [2], we focus on the TA-SCBT scheme in this paper. The goal is to develop a high-performance, low-complexity equalizer for TA-SCBT.

In [1], frequency-domain (FD) linear equalizer (LE) was proposed to mitigate ISI. Although it has a very low complexity, the performance leaves much room for improvement due to the effect of noise enhancement. Subsequently, the hybrid DFE (HDFE) was proposed in [3], in which the FD feedforward filter (FFF) is combined with the TD feedback filter (FBF) to ameliorate the noise enhancement effect. However, the performance gap between HDFE and the matched-filter bound (MFB), a performance lower bound, is still quite large. To improve the performance, sequence detection can be used. Although the maximum-likelihood sequence detector is the optimal solution, the huge complexity makes it impractical for SCBT systems. In [4], the suboptimal sequence detector using the QRD-M algorithm was proposed to equalize the SCBT signals, showing a considerable performance gain over HDFE. However, it does not lend itself to efficient FD processing; as a result, the complexity is unnecessarily high. In this paper, we propose a tree search equalizer that overcomes such a drawback; it consists of a FD prefilter followed by the M-algorithm. By properly designing the prefilter, the proposed algorithm is far more efficient than the QRD-M algorithm, while maintaining almost the same detection performance.

The rest of the paper is organized as follows. Section 2 describes the signal model. Section 3 reviews the QRD-M algorithm that serves as the baseline for comparison in terms of performance and complexity. The proposed algorithms and the simulation results are discussed in Sections 4 and 5, respectively. Unless otherwise mentioned, the k-th entry of a vector $\mathbf{x}$ is denoted as x_k.

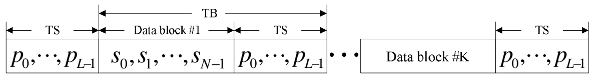

Fig. 1. The block structure of TA-SCBT.

2. SIGNAL MODEL

Fig. 1 shows the block structure of TA-SCBT. Each transmission block (TB) consists of a data block followed by a TS. The data block $\mathbf{s} \triangleq [s_0, \ldots, s_{N-1}]^T$ consists of modulation symbols taken independently from a constellation. Denoted as $\mathbf{p} \triangleq [p_0, \ldots, p_{L-1}]^T$, the TS, whose contents are known at the receiver, is appended to each data block to serve as the GT between adjacent data blocks. We can therefore express one TB as

$$\begin{aligned} \mathbf{x} &\triangleq [x_0, \ldots, x_{B-1}]^T \\ &= [\mathbf{s}^T \mathbf{p}^T]^T \end{aligned} \tag{1}$$

where $B{=}N{+}L$ is the length of the TB. As shown in Fig. 1, one extra TS is placed in front of the first TB. Moreover, the same TS is used in all the GTs. As a result, the TS preceding any TB serves as the CP of that TB. We assume that each entry of $\mathbf{x}$ is of zero mean and of a variance of σ_x^2, and that entries of $\mathbf{x}$ are independent.

Supported by the National Science Council, Taiwan, R.O.C., under contract NSC 101-2221-E-006-174-MY2.

We assume that the equivalent discrete-time channel impulse response (CIR) is causal, and is time-invariant over one TB. Denote the CIR as $\mathbf{h} \triangleq [h_0, \ldots, h_{L_h-1}, 0, \ldots, 0]^T$ where the support of $\mathbf{h}$ is denoted as L_h. For convenience, we have zero padded the CIR to be a $B\times 1$ vector, i.e., $h_i=0$ for $i\geq L_h$. We further assume that $L_h \leq L+1$ such that no IBI incurs. It follows that, with symbol-rate sampling, the i-th received sample of the TB is given by

$$y_i=h_i \otimes x_i + n_i, \qquad i=0,\ldots,B-1, \tag{2}$$

where $\otimes$ denotes the circular convolution operation, and n_i is the noise component. Alternatively, the received block, defined as $\mathbf{y} \triangleq [y_0, \ldots, y_{B-1}]^T$, can be written as

$$\mathbf{y}=\mathbf{H}_{\mathrm{c}}\mathbf{x}+\mathbf{n} \tag{3}$$

where the channel matrix $\mathbf{H}_{\mathrm{c}}$, given by

$$\mathbf{H}_{\mathrm{c}} = \begin{bmatrix} h_0 & & & h_{L_h-1} \cdots & h_1 \\ h_1 & h_0 & & \ddots & \vdots \\ \vdots & \vdots & \ddots & & h_{L_h-1} \\ h_{L_h-1} & \vdots & h_0 & \mathbf{0} & \\ & h_{L_h-1} & & \ddots & \\ & & \ddots & \ddots & \\ \mathbf{0} & & h_{L_h-1} & \cdots \; h_1 & h_0 \end{bmatrix}, \tag{4}$$

is a circulant matrix whose first column is $\mathbf{h}$, and we assume that the noise vector $\mathbf{n} \triangleq [n_0, \ldots, n_{B-1}]^T \sim \mathcal{CN}(\mathbf{0}, \sigma_n^2 \mathbf{I})$. For convenience, we define the order of a circulant matrix as the support of its first column; hence, $\mathbf{H}_{\mathrm{c}}$ is an L_h-th order circulant matrix.

Since the eigenvalue decomposition of any circulant matrix $\mathbf{H}_{\mathrm{c}}$ is given by

$$\mathbf{H}_{\mathrm{c}}=\mathbf{F}^H \mathbf{\Lambda}_H \mathbf{F} \tag{5}$$

where $\mathbf{F}$ is the $B\times B$ unitary discrete Fourier transform (DFT) matrix (i.e., $\mathbf{F}^H\mathbf{F}=\mathbf{F}\mathbf{F}^H=\mathbf{I}$), and $\mathbf{\Lambda}_H$ is a diagonal matrix with the k-th diagonal element given by $H_k=\sum_{l=0}^{L_h-1} h_l e^{-j2\pi kl/B}$, $k=0,\ldots,B-1$, the FD received block, defined as $\mathbf{y}_{\mathrm{F}} \triangleq \mathbf{F}\mathbf{y}$, can be written, using (3) and (5), as

$$\mathbf{y}_{\mathrm{F}}=\mathbf{\Lambda}_H\mathbf{F}\mathbf{x}+\mathbf{n}_{\mathrm{F}}, \tag{6}$$

where $\mathbf{n}_{\mathrm{F}} \triangleq \mathbf{F}\mathbf{n}$ has the same distribution as $\mathbf{n}$.

3. REVIEW OF QRD-M ALGORITHM

Let the QR decomposition (QRD) of $\tilde{\mathbf{H}} \triangleq \mathbf{\Lambda}_H\mathbf{F}$, the equivalent channel matrix in (6), be $\tilde{\mathbf{H}}=\mathbf{Q}\mathbf{R}$, where $\mathbf{Q}$ is an $B\times B$ unitary matrix, and $\mathbf{R}$ is an upper triangular matrix. Multiplying $\mathbf{y}_{\mathrm{F}}$ by $\mathbf{Q}^H$ on the left, we obtain

$$\mathbf{z} \triangleq \mathbf{Q}^H\mathbf{y}_{\mathrm{F}}=\mathbf{R}\mathbf{x}+\mathbf{n}' \tag{7}$$

where $\mathbf{n}' \triangleq \mathbf{Q}^H\mathbf{n}_{\mathrm{F}}$ can be shown to be $\mathcal{CN}(\mathbf{0}, \sigma_n^2\mathbf{I})$. Note that the last L elements of $\mathbf{z}$ are irrelevant to detecting $\mathbf{s}$ because they do not depend on $\mathbf{s}$ and, in addition, noise samples are independent. Therefore, (7) can be reduced to

$$\bar{\mathbf{z}}=\bar{\mathbf{R}}\mathbf{s}+\bar{\mathbf{n}}' \tag{8}$$

where $\bar{\mathbf{z}} \triangleq [\bar{z}_0, \ldots, \bar{z}_{N-1}]^T$, $\bar{z}_i \triangleq z_i - \sum_{j=0}^{L-1} r_{i,N+j}p_j$, $r_{i,j}$ denotes the (i,j)-th entry of $\mathbf{R}$, $\bar{\mathbf{R}}$ is the $N\times N$ matrix taken from the upper-left corner of $\mathbf{R}$, and $\bar{\mathbf{n}}'$ consists of the first N entries of $\mathbf{n}'$.

Since $\bar{\mathbf{R}}$ in (8) is a (upper) triangular matrix, the M-algorithm can be readily applied to $\bar{\mathbf{z}}$; it searches over a tree of $N+1$ levels in an efficient manner to arrive at the decision on $\mathbf{s}$. Starting from the root node (i.e., level 0), each node at level $i-1$ ($i=1,\ldots,N$) stems out $|C|$ branches (which lead to $|C|$ child nodes, respectively, at level i). Each branch represents a distinct hypothesis on symbol s_{N-i}, and is assigned a branch metric (BM), defined as

$$\beta_i = \left| \bar{z}_{N-i} - \sum_{m=N-i}^{N-1} \bar{r}_{N-i,m}s_m \right|^2, \quad i=1,\ldots,N, \tag{9}$$

where $\bar{r}_{k,j}$ is the (k,j)-th entry of $\bar{\mathbf{R}}$. Each path that starts at the root node and ends at a node at level i represents a particular symbol vector hypothesis $\mathbf{s}_i \triangleq [s_{N-1}, \ldots, s_{N-i}]$. Each path is associated with a path metric (PM), defined as $\gamma_i(\mathbf{s}_i) \triangleq \sum_{j=1}^{i} \beta_j$. When the M-algorithm proceeds from level $i-1$ to level i, all the existing $(i-1)$-branch paths are extended to level i. The PMs of the extended paths are computed; only the best M extended paths (i.e., those whose PMs are ranked among the M smallest) are retained. This process is repeated until it reaches level N; the N-branch path with the minimum PM then gives the QRD-M solution.

4. PROPOSED ALGORITHM

QRD-M (with $M>1$) significantly outperforms HDFE, at the cost of a dramatic increase in complexity. Our analysis indicates that the overall complexity of QRD-M is dominated by that of QRD, which is used to generate the tree structure (manifested by the upper triangular matrix $\mathbf{R}$, or, equivalently, $\bar{\mathbf{R}}$). In this section, we describe a much more efficient tree search equalizer. We first describe in Section 4.1 an approach that enables tree search equalization without QRD. The proposed algorithm, extending this approach while rectifying the performance loss of it, is developed in Section 4.2.

4.1. Motivation: Tree search without QRD

Using the partitioned forms (1) and $\mathbf{H}_{\mathrm{c}} \triangleq [\mathbf{H}_{\mathrm{s}}\ \mathbf{H}_{\mathrm{p}}]$ where $\mathbf{H}_{\mathrm{s}}$ and $\mathbf{H}_{\mathrm{p}}$ consist of the first N and the last L columns of $\mathbf{H}_{\mathrm{c}}$, respectively, we can rewrite (3) as $\mathbf{y}=\mathbf{H}_{\mathrm{s}}\mathbf{s}+\mathbf{H}_{\mathrm{p}}\mathbf{p}+\mathbf{n}$. Assuming perfect channel knowledge at the receiver, the contribution of TS can be removed from $\mathbf{y}$, giving

$$\bar{\mathbf{y}} \triangleq \mathbf{y}-\mathbf{H}_{\mathrm{p}}\mathbf{p} = \mathbf{H}_{\mathrm{s}}\mathbf{s}+\mathbf{n}. \tag{10}$$

Observe that the entries above the main diagonal of $\mathbf{H}_{\mathrm{s}}$ are identically zeros. Therefore, the M-algorithm can be carried out on $\bar{\mathbf{y}}$ based on (10), without QRD; the only modification needed is that the definitions of BMs be changed to:

$$\beta_i = \begin{cases} \left| \bar{y}_{i-1} - \sum_{m=1}^{i} h_{i-m}s_{m-1} \right|^2, & i=1,\ldots,N-1, \\ \sum_{l=N}^{N+L_h-1} \left| \bar{y}_{l-1} - \sum_{m=1}^{N} h_{l-m}s_{m-1} \right|^2, & i=N. \end{cases} \tag{11}$$

We note the following. First, this approach is valid if $L_h \leq L+1$ (which is true under the condition of no IBI). Second, by exploiting the circulant structure of $\mathbf{H}_{\mathrm{c}}$ and the presence of TS, this approach does not require QRD. For convenience, we refer to this approach as the direct M-algorithm (DM). It is clear that DM achieves a much lower complexity than QRD-M, if both algorithms use the same value of M. However, simulation results show that, if the same value of M used is modest (e.g., $M{=}1, 2, 4$, or 8, etc.), the detection performance of DM lags significantly behind that of QRD-M. The cause of such a performance loss is illustrated in Section 4.1.1.

4.1.1. *Performance Loss in DM Algorithm*

Let us define the pruning probability of a tree search detector employing the M-algorithm, denoted by $\mathrm{P}_{\mathrm{prune}}(M{=}i)$, as the probability that the correct hypothesis is removed *at the first tree level (i.e., level 1)* when $M{=}i$ is adopted for the M-algorithm. Consider the signal processed by DM at the first tree level, given by $\bar{y}_0{=}h_0x_0{+}n_0$. It can be shown that, if QPSK is used,

$$\begin{aligned}\mathrm{P}^{(\mathrm{DM})}_{\mathrm{prune}}(M{=}1) &= 2Q(\sqrt{\mathrm{CSNR}_{\mathrm{DM}}}){-}Q^2(\sqrt{\mathrm{CSNR}_{\mathrm{DM}}}), \\ &\approx 2Q(\sqrt{\mathrm{CSNR}_{\mathrm{DM}}}), \qquad (12)\end{aligned}$$

$$\mathrm{P}^{(\mathrm{DM})}_{\mathrm{prune}}(M{=}2){=}Q(\sqrt{2\mathrm{CSNR}_{\mathrm{DM}}}), \qquad (13)$$

and

$$\mathrm{P}^{(\mathrm{DM})}_{\mathrm{prune}}(M{=}3){=}Q^2(\sqrt{\mathrm{CSNR}_{\mathrm{DM}}}), \qquad (14)$$

where $Q(\nu)\triangleq 1/\sqrt{2\pi}\int_{\nu}^{\infty}e^{-\epsilon^2/2}d\epsilon$. Here, $\mathrm{CSNR}_{\mathrm{DM}}\triangleq\frac{|h_0|^2\sigma_x^2}{\sigma_n^2}$ represents the cursor signal-to-noise ratio (CSNR), because h_0 corresponds to the cursor of $\mathbf{h}$. Note that the approximation in (12) is valid for moderate to high CSNRs. For QRD-M, on the other hand, the signal processed at the first tree level is given by $\bar{z}_{N-1}{=}\bar{r}_{N-1,N-1}x_{N-1}{+}\bar{n}'_{N-1}$. Therefore, the expression of $\mathrm{P}^{(\mathrm{QRD-M})}_{\mathrm{prune}}(M{=}i)$ is the same as that of $\mathrm{P}^{(\mathrm{DM})}_{\mathrm{prune}}(M{=}i)$, except that $\mathrm{CSNR}_{\mathrm{DM}}$ is replaced by $\mathrm{CSNR}_{\mathrm{QRD-M}}\triangleq\frac{|\bar{r}_{N-1,N-1}|^2\sigma_x^2}{\sigma_n^2}$. It follows from (12) – (14) that, for any $M{<}|C|$, a lower CSNR gives a higher pruning probability, leading to a poorer detection performance as error propagation is more likely to occur. Note that similar results can be obtained for q-ary squared QAMs (for $q = 4{\cdot}2^{2\lambda}$, where λ is any non-negative integer.)

Fig. 2 plots $\mathrm{CSNR}_{\mathrm{DM}}$ and the corresponding $\mathrm{CSNR}_{\mathrm{QRD-M}}$ for 1000 independent realizations of $\mathbf{H}_{\mathrm{c}}$ (i.e., each $\mathbf{R}$ is obtained from the respective $\mathbf{H}_{\mathrm{c}}$) at a channel SNR (or, simply, SNR), defined as $\mathrm{SNR}\triangleq\frac{\sigma_x^2}{\sigma_n^2}$, of 10 dB. The channel model is specified in Section 5. It is clear that DM operates at a lower CSNR than QRD-M, which explains the performance loss.

4.2. Proposed FDF-M Algorithm

Fig. 3 illustrates the scheme we proposed to overcome the performance loss of DM. The received signal is processed by the prefilter $\mathbf{G}^H$ (designed to enhance the CSNR) before invoking the DM algorithm. Using (3), the input of the DM algorithm is thus given by

$$\mathbf{v}\triangleq\mathbf{G}^H\mathbf{y}{=}\mathbf{U}_{\mathrm{c}}\mathbf{x}{+}\mathbf{w} \qquad (15)$$

where $\mathbf{U}_{\mathrm{c}}\triangleq\mathbf{G}^H\mathbf{H}_{\mathrm{c}}$ denotes the effective channel seen by DM and $\mathbf{w}\triangleq\mathbf{G}^H\mathbf{n}$ is the filtered noise. In designing $\mathbf{G}^H$, we impose the following two constraints. First, in order to be compatible with DM, we require that $\mathbf{U}_{\mathrm{c}}$ be an L_u-th order circulant matrix with L_u satisfying $L_u{\le}L{+}1$. (Note that L_u is a user-specified parameter.) Consequently, denoting the first column of $\mathbf{U}_{\mathrm{c}}$ as $\mathbf{u}\triangleq[u_0,\ldots,u_{L_u-1},0,\ldots,0]^T$, we have $v_i{=}u_i{\otimes}x_i{+}w_i$, $i{=}0,\ldots,B{-}1$, where $\mathbf{u}$ represents the impulse response of the effective channel. Second, the CSNR that is seen by DM is maximized for the chosen L_u.

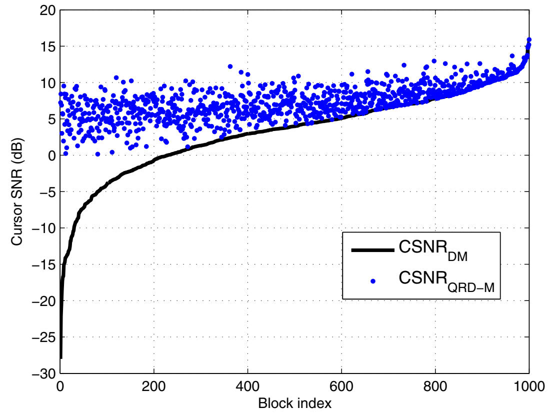

Fig. 2. Comparison of $\mathrm{CSNR}_{\mathrm{DM}}$ and $\mathrm{CSNR}_{\mathrm{QRD-M}}$ for 1000 independent realizations of $\mathbf{H}_{\mathrm{c}}$.

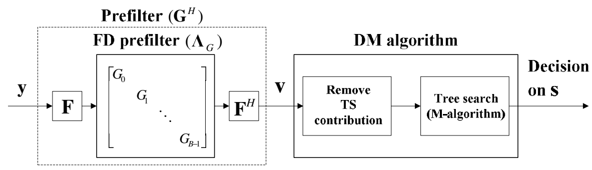

Fig. 3. Proposed equalizer structure: the FDF-M algorithm.

Since $\mathbf{U}_{\mathrm{c}}$ and $\mathbf{H}_{\mathrm{c}}$ are both circulant, it follows that $\mathbf{G}^H$ is also circulant. We can therefore decompose $\mathbf{G}^H$ into $\mathbf{G}^H{=}\mathbf{F}^H\mathbf{\Lambda}_G\mathbf{F}$ where $\mathbf{\Lambda}_G$ is a diagonal matrix whose i-th diagonal element is denoted as G_i. This leads to the FD implementation of the prefilter (see Fig. 3) that reduces the signal processing complexity of prefiltering from $O(B^2)$, assuming being implemented in TD, to $O(B\log_2 B)$. The proposed algorithm is thus referred to as FDF-M, standing for FD filtering followed by the M-algorithm. Note that the diagonal of $\mathbf{\Lambda}_G$ represents the frequency response of the prefilter.

4.2.1. *Derivation of FD Prefilter Coefficients*

Let us denote the FD prefilter coefficients (to be determined in the following) as $\mathbf{g}_{\mathrm{F}}\triangleq[G_0,\ldots,G_{B-1}]^T$. Since $\mathbf{U}_{\mathrm{c}}{=}\mathbf{F}^H\mathbf{\Lambda}_G\mathbf{\Lambda}_H\mathbf{F}$ (using (5)), it follows that $\sqrt{B}\mathbf{F}\mathbf{u}{=}\mathbf{\Lambda}_H\mathbf{g}_{\mathrm{F}}$. Assuming that $\mathbf{\Lambda}_H$ is invertible (i.e., $H_k{\neq}0, \forall k\in[0,B{-}1]$), we have

$$\mathbf{g}_{\mathrm{F}}{=}\sqrt{B}\mathbf{\Lambda}_H^{-1}\mathbf{F}\mathbf{u}. \qquad (16)$$

It can be shown that w_i is $\mathcal{CN}(0,\frac{\sigma_n^2}{B}\|\mathbf{g}_{\mathrm{F}}\|^2)$. From (15), therefore, the CSNR of FDF-M is given by

$$\mathrm{CSNR}_{\mathrm{FDF-M}}\triangleq\frac{|u_0|^2\sigma_x^2}{\frac{\sigma_n^2}{B}\|\mathbf{g}_{\mathrm{F}}\|^2}{=}\frac{|u_0|^2\sigma_x^2}{\sigma_n^2\left\|\mathbf{\Lambda}_H^{-1}\mathbf{F}\mathbf{u}\right\|^2}. \qquad (17)$$

Without loss of generality, we can set $u_0{=}1$. Rewriting $\mathbf{u}$ as $\mathbf{u}{=}[1,\tilde{\mathbf{u}},0,\ldots,0]^T$ where $\tilde{\mathbf{u}}\triangleq[u_1,\ldots,u_{L_u-1}]^T$ and plugging into (17), we arrive at

$$\mathrm{CSNR}_{\mathrm{FDF-M}}{=}\frac{\sigma_x^2}{\sigma_n^2\left\|\mathbf{\Lambda}_H^{-1}(\frac{1}{\sqrt{B}}\mathbf{1}{+}\tilde{\mathbf{F}}\tilde{\mathbf{u}})\right\|^2} \qquad (18)$$

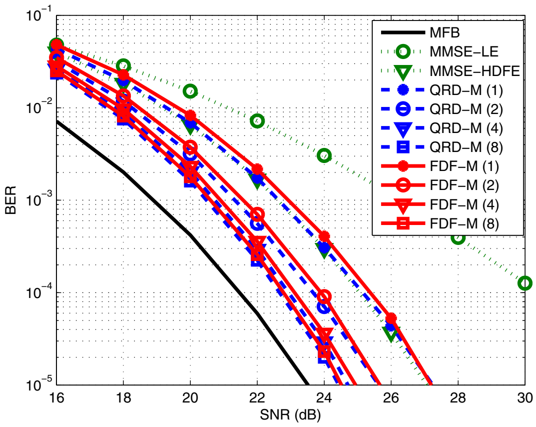

Fig. 4. Comparison of BER performance. 16-QAM is used.

where $\tilde{\mathbf{F}}$ consists of the second to L_u-th columns of $\mathbf{F}$, and $\mathbf{1}$ is the all-one vector of length B. From (18), it can be shown that the optimum $\tilde{\mathbf{u}}$ that maximizes $\mathrm{CSNR}_{\mathrm{FDF-M}}$ is given by $\tilde{\mathbf{u}}=-\mathbf{A}^{-1}\mathbf{b}$, where $\mathbf{A} \triangleq \tilde{\mathbf{F}}^H \mathbf{\Lambda}_H^{-1}\mathbf{\Lambda}_H^{-H}\tilde{\mathbf{F}}$ and $\mathbf{b} \triangleq \frac{1}{\sqrt{B}}\tilde{\mathbf{F}}^H \mathbf{\Lambda}_H^{-1}\mathbf{\Lambda}_H^{-H}\mathbf{1}$. Once the optimum $\tilde{\mathbf{u}}$ (and, hence, the optimum $\mathbf{u}$) is determined, the FD prefilter coefficient $\mathbf{g}_{\mathrm{F}}$ can be obtained via (16).

It should be noted that $\tilde{\mathbf{u}}$ can be solved via the Levinson algorithm, which takes a complexity of $O(L_u^2)$. Besides, $\mathbf{A}$, $\mathbf{b}$, and (16) can be efficiently computed through the fast Fourier transform. In contrast, $\mathbf{Q}^H$, the prefilter for QRD-M, is obtained via QRD, which takes a complexity of $O(B^3)$. Therefore, computing the prefilter of FDF-M has a much lower complexity than that of QRD-M.

5. SIMULATION RESULTS

The channel model we simulated takes on the exponentially-decaying power delay profile. Each tap gain h_l, $l{=}0,\ldots,L_h{-}1$ is an independent $\mathcal{CN}(0,\sigma_l^2)$. In addition, we assume that $E\{\|\mathbf{h}\|^2\}{=}1$ (i.e., $\sum_{l=0}^{L_h-1}\sigma_l^2{=}1$), and that $\{\sigma_l^2\}$ results in a root mean square delay spread of two symbol periods. The channel length is set to be $L_h{=}16$. In the simulations, $\mathbf{h}$ was held constant within each interval of a TB, but was independently generated for different TBs. We assume that the channel estimates are perfect at the receiver. The parameters of the TB are given by $B{=}64$, $N{=}48$, and $L{=}16$. We set $L_u{=}16$ (i.e., $L_u{=}L_h$) for FDF-M. For the purposes of comparison, we simulated HDFE and FD-LE as well, both under the criterion of minimum mean square error (MMSE); we refer to them as MMSE-HDFE and MMSE-LE, respectively. For MMSE-HDFE, we set the length of FBF to be 16 (taps).

5.1. Detection Performance

Fig. 4 compares the bit-error-rate (BER) performance in the case of 16-QAM. The MFB is also plotted for reference. Observe that FDF-M performs very closely to QRD-M, when both use the same value of M. As M increases, the performance of FDF-M and QRD-M improve; however, when $M{>}4$, the performance improvement is diminishing. Therefore, we use $M{=}4$ when comparing complexity in Section 5.2. In addition, observe that, at a BER of about 10^{-4}, FDF-M (with $M{=}4$) performs about 7 dB and 2 dB, respectively, better than MMSE-LE and MMSE-HDFE. Although not shown here due to space limit, simulation results indicate that similar observations can also be made for BPSK, QPSK, and 64-QAM.

Equalizer	BPSK	QPSK	16-QAM	64-QAM
QRD-M ($M{=}4$)	274026	276756	293136	358656
FDF-M ($M{=}4$)	1844	2372	5540	18212
MMSE-HDFE	1346	1376	1556	2276

Table 1. Comparison of complexity in terms of the number of complex-valued multiplications required to equalize a single block.

5.2. Complexity

Table 1 compares the complexity in terms of the number of complex-valued multiplications required to equalize a single block, for the same scenario specified in Section 5. The complexity number accounts for the following: (i) prefilter design (i.e., computing the prefilter or FFF coefficients, respectively), (ii) preprocessing (i.e., prefiltering and removing the contribution of TS for QRD-M and FDF-M, or running FFF for MMSE-HDFE), and (iii) detection (i.e., performing M-algorithm or running FBF, respectively). Note that we assume that, for both FDF-M and QRD-M, the lookup table implementation [5] is adopted in computing the BMs. It is clear from Table 1 that FDF-M has a significantly lower complexity than QRD-M. On the other hand, the complexity increase of FDF-M with respect to MMSE-HDFE is modest.

6. CONCLUSION

In this paper, we proposed a tree search equalizer, referred to as the FDF-M algorithm, for TA-SCBT systems. It is comprised of a prefilter followed by the M-algorithm. The prefilter was designed to condition the channel, while preserving the circulant channel structure that facilitates tree search detection and enables efficient FD implementation. Unlike QRD-M, FDF-M possesses typical implementation advantages of FDE, thereby achieving a far better performance-complexity tradeoff than QRD-M.

7. REFERENCES

[1] D. Falconer, S. L. Ariyavisitakul, A. Benyamin-Seeyar, and B. Eidson, "Frequency domain equalization for single-carrier broadband wireless systems," *IEEE Communications Magazine*, vol. 40, no. 4, pp. 58–66, Apr. 2002.

[2] L. Deneire, B. Gyselinckx, and M. Engels, "Training sequence versus cyclic prefix – a new look on single carrier communication," *IEEE Communications Letters*, vol. 5, no. 7, pp. 292–294, July 2001.

[3] N. Benvenuto and S. Tomasin, "On the comparison between OFDM and single carrier modulation with a DFE using a frequency-domain feedforward filter," *IEEE Trans. on Communications*, vol. 50, no. 6, pp. 947–955, June 2002.

[4] T. Yamamoto, K. Takeda, and F. Adachi, "Frequency-domain block signal detection with QRM-MLD for training sequence-aided single-carrier transmission," *EURASIP Journal on Advances in Signal Processing*, vol. 2011, 2011.

[5] H. Kawai, K. Higuchi, N. Maeda, and M. Sawahashi, "Adaptive control of surviving symbol replica candidates in QRM-MLD for OFDM MIMO multiplexing," *IEEE Journal on Selected Areas in Communications*, vol. 24, pp. 1130–1140, June 2006.